

Fabrication of a nanocomposite from an agricultural waste and its application as a biosorbent for organic pollutants

S. M. Ali^{1,2}

Received: 17 April 2017/Revised: 18 June 2017/Accepted: 19 July 2017/Published online: 2 August 2017
© Islamic Azad University (IAU) 2017

Abstract Cellulose/SiO₂ nanocomposite (CSNC) was successively prepared using a banana peel waste as a template for silica. X-rays diffraction confirmed the presence of both cellulosic and silica phases with the silica phase as the primary phase. Electron microscopes images showed a compact hexagonal morphology with an average particle size of 20 nm. The FTIR analysis ascertained the presence of hydroxyl groups, and the thermal analysis showed the high thermal stability of CSNC. The sorption ability of CSNC for methylene blue was examined in both aqueous solutions and a real sample. The adsorption was followed by pseudo-second-order reaction and obeyed Langmuir isotherm. Calculated thermodynamic parameters showed that the adsorption is spontaneous and exothermic, suggesting a chemisorption mode. The calculated adsorption capacity was 78.75 and 58.81 mg g⁻¹ in aqueous dye solution and real sample, respectively, suggesting the applicability of CSNC for field uses. The correlation between the composite components and its performance is suggested to be investigated in the future by changing the type of agricultural waste as well as the nanooxide.

Keywords Nanocomposite · Biological waste · Adsorption · Water decontamination

Introduction

Organic dyes can be considered a major water pollution source, as it is used in different industrial processes. Methylene blue (MB) is one of the most common dyes, which establishes a dangerous component in many industrial effluents. Various methods can be employed for the dye removal such as adsorption, chemical oxidation, electrochemical techniques, and biological routes (Hashemian and Foroghimoqhadam 2014). Adsorption has the advantages of being simple, insensitive to other toxic substance, and easily recovers from the adsorbent (Crini 2006). Several agricultural wastes have been employed as biosorbents for dye removal such as banana and orange peels (Anadurai et al. 2002), peanut hull (Gong et al. 2005), grass waste (Hameed 2009), rice husk (Vadivelan and Kumar 2005), and mango seed kernel (Kumar and Kumaran 2005).

Naturally, banana peel (BP) has been successively used as a sorbent for many inorganic and organic pollutants due to the presence of hydroxyl groups which can strongly bind these compounds and offer a possible route for its removal (Anastopoulos and Kyzas 2014). The adsorption of MB from aqueous solutions by BP can be improved by an electrocoagulation/adsorption coupling process (Carvalho et al. 2015). Introducing more active functional groups can further enhance the sorbent efficiency which can be done by chemical modification. Chemically modified BP was used for the removal of the MB dye by Amela et al. (2012). The maximum adsorption capacities for activated BP and natural BP were 19.67 and 18.65 mg g⁻¹ at pH 4–8, 20 °C. In addition, Mn(II) (Ali 2017), Cr(VI) (Ali et al. 2016), Cu(II), Ni(II), and Pb(II) ions (Thuan et al. 2017) have been removed by the chemically modified BP.

Nanocomposites prepared from biological materials have recently attracted the interest of many scientists' due

Editorial responsibility Agnieszka Galuszka.

✉ S. M. Ali
dr_shimaaali80@yahoo.com

¹ Department of Chemistry, Faculty of Science, Taibah University, Madinah 30002, Kingdom of Saudi Arabia

² Department of Chemistry, Faculty of Science, Cairo University, Giza 12613, Egypt

to their wide range of applications and its effective cost (Anastopoulos and Kyzas 2015; Kyzas and Matis 2015). The conversion of cellulosic wastes such as sugarcane, wastepaper, and sawdust into nanocomposites by being mixed with nanooxides and then calcinated has been reported (Pang et al. 2011). Nanowood-based materials were successively synthesized by the sol–gel process (Mamoru et al. 2005; Ota et al. 2000). Natural cellulose can be infiltrated with metal chlorides which upon heating can be transformed into metal oxides nanofibers (Patel and Padhi 1993; Cao et al. 2004). Nanocellulosic material was prepared from micro-sized banana fibers by a high-energy ball milling (Nagendra et al. 2014). It was found that the particle size decreased sharply with the milling's time and the milling ball energy. Cellulose nanofibers were successively isolated by Pelissari et al. from BP using chemical and enzymatic treatment (Tibolla et al. 2014). Another route to form nano-BP has been proceeded via acid hydrolysis of natural BP followed by xanthation to introduce sulfur-containing functional groups (Pillai et al. 2013). Xanthated nano-BP showed a high biosorption capacity for Cd(II) ions from aqueous solutions. The use of nanocomposites as efficient sorbents for MB was also reported, for example, silica-based nanocomposites (Chen et al. 2016; Wu et al. 2016b), γ -Fe₂O₃/graphene (Song et al. 2015), and MIL-100(Fe) (Tan et al. 2015).

In the present work, cellulose/SiO₂ nanocomposite (CSNC) will be prepared by using BP wastes as a template for inorganic silicon oxide. The prepared nanocomposite will be characterized and applied as a biosorbent for MB removal from aqueous solutions and wastewater. Kinetics and thermodynamic parameters will be calculated, and possible adsorption mechanism will be investigated.

Materials and methods

Materials

Tetraethylorthosilicate, absolute ethanol (99.8%), ammonium hydroxide (33%), and nitric acid (69%) were purchased from Sigma-Aldrich. Methylene blue (C₁₆H₁₈N₃SCI) was bought from Brixworth, Northants, UK.

Preparation of CSNC

Nanosilica was first synthesized via the alkaline hydrolysis of tetraethylorthosilicate in ethanol medium (Rao et al. 2005). BP was washed to remove any contaminants, placed at 80 °C for 3 days to remove moisture, and crushed; then, 10 g of BP powder was added to 50 mL of suspended silica solution, shaken for 16 h at 135 rpm, filtrated, placed at 80 °C for 3 h, and calcinated at 550 °C for 1 h (Pang et al. 2011).

Adsorption experiment

MB solutions used in adsorption experiments were diluted from a stock solution (1000 mg L⁻¹) to the required concentrations. The removal of MB by CSNC was carried out by adding 0.05 g of the composite into 25 mL of MB solution at optimum pH. Then, the samples were shaken at a constant speed of 135 rpm at 25 °C for 24 h and were centrifuged at 3500 rpm for 1 h. The undesorbed MB concentration was determined using UV–Vis spectrometer (Evolution 300 UV–Vis, Thermo scientific, Germany) at $\lambda_{\max} = 665$ nm. The removal percentage of dye can be calculated according to:

$$(\text{Removal } \%) = \frac{C_0 - C_e}{C_0} \times 100 \quad (1)$$

The equilibrium adsorbed MB amount, q_e (mg g⁻¹), is given by:

$$q_e = \frac{(C_0 - C_e)V}{W} \quad (2)$$

where C_0 and C_e are initial and equilibrium dye concentrations (mg L⁻¹), respectively, V is the solution volume (L), and W is the sorbent weight (g).

Adsorption kinetics

The adsorption kinetics were evaluated using different models (Ansari and Dezhmpanah 2013).

Pseudo-first-order

$$\log(q_e - q_t) = \log q_e - \frac{K1}{2.303} t \quad (3)$$

where q_e and q_t are adsorbed amounts of dye (mg g⁻¹) on the presented composite at equilibrium, and at time t (min), respectively. $K1$ is the rate constant of the first-order adsorption.

Pseudo-second-order

$$\frac{t}{q_t} = \frac{1}{K2q_e} + \frac{t}{q_e} \quad (4)$$

where $K2$ is the rate constant of the second-order adsorption.

Thermodynamics equations

According to the transition-state equation (Ansari and Dezhmpanah 2013):

$$\ln K_c = \frac{\Delta S}{R} - \frac{\Delta H}{R} \left(\frac{1}{T} \right) \quad (5)$$

$$K_c = \frac{C_{Ad}}{C_e} \quad (6)$$

where K_c is the equilibrium constant, C_{Ad} is the equilibrium adsorbed dye amount (mg L^{-1}), C_e is the dye equilibrium concentration (mg L^{-1}), R is the gas constant ($8.314 \text{ J mol}^{-1} \text{ K}^{-1}$), and T is the temperature (K).

Arrhenius equation (Al-Rashed and Al-Gaid 2012):

$$\ln K_2 = -\frac{E_a}{RT} + \ln A \quad (7)$$

where E_a is the activation energy (kJ mol^{-1}), A is the Arrhenius temperature-independent factor, and K_2 is the second-order rate constant.

Adsorption isotherms

The linear equation of Langmuir model is represented by Jebreil (2014):

$$\frac{C_e}{q_e} = \frac{1}{q_{mb}} + \frac{C_e}{q_m} \quad (8)$$

where q_m is maximum amount sorbed (mg g^{-1}) when the monolayer is complete. K_L is Langmuir constant (L mg^{-1}).

Freundlich model is given as (Dawood and Sen 2012):

$$\ln q_e = \ln K_f + \frac{1}{n} \ln C_e \quad (9)$$

where K_f and n are isotherm constants.

Structural, surface, and thermal characterizations

The phase identification is carried out by using X-ray diffractograms (XRD, Shimadzu, XRD-7000, Japan) at 40 kV and 30 mA, using CuK_α incident beam ($\lambda = 0.154 \text{ nm}$). The scanning range of 2θ is set between 20° and 80° .

The surface morphology is observed by using scanning electron microscope (SEM, Superscan SS-550, Shimadzu, Japan) and transmission electron microscopy (TEM, JEOL JEM 1400, Japan).

The functional groups are characterized by FTIR (FTIR, IRAffinity-1S, Shimadzu, Japan). TGA is performed by using Q600 TA Instruments under N_2 atmosphere; heating rate is $10 \text{ }^\circ\text{C min}^{-1}$, to investigate the thermal stability of samples.

Results and discussion

Characterization of natural BP and the prepared CSNC

Figure 1 shows XRD patterns of BP and CSNC. A peak appears at $2\theta = 22^\circ$, characteristic of the cellulosic plane (002) for both samples (Pereira et al. 2013). An additional

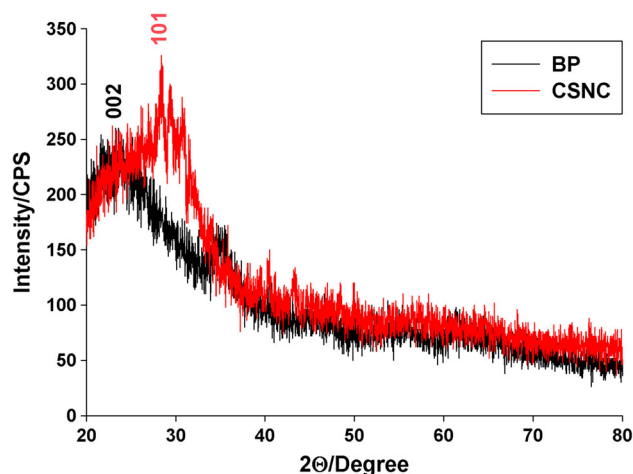


Fig. 1 X-rays diffraction (XRD) spectra of banana peel (BP) and cellulose/SiO₂ nanocomposite (CSNC); peaks of cellulose and silica phases are indexed

peak at $2\theta = 28^\circ$ is observed for CSNC samples, corresponding to (101) the plane of amorphous hexagonal phase silica as compared with silica ICDD card number 00-011-0252 and as reported by Ferreira et al. (2015). This peak is also the major peak which means that silica constitutes the primary phase of CSNC sample. CSNC has low crystallinity as indicated by the low peaks intensities.

The BET surface area values for BP and CSNC were determined by the N_2 adsorption isotherm. It is found that BET surface area of BP is $1.9 \text{ m}^2 \text{ g}^{-1}$, with an average pore size of 1.02 nm. On the other hand, the BET surface area of CSNC is $8.9 \text{ m}^2 \text{ g}^{-1}$, with an average pore size of 1.56 nm. Thus, the proposed modification of BP increased its surface area value by about four times with a slight increase in the average pore size.

TEM images for both BP and CSNC are presented in Fig. 2. A tissue-like morphology was assigned for the natural BP sample, Fig. 2a. On the other hand, CSNC showed hexagonal shaped particles, Fig. 2b, with an average particle size of about 20 nm. SEM images for BP and CSNC are presented in Fig. 2c, d, respectively. The morphology of BP consists of compact folded paper morphology, while hexagonal grains are characteristic of CSNC.

Structural characterization by FTIR was performed to identify the functional groups in both BP and CSNC samples, Fig. 3a. For the BP sample, a broad peak at 3400 cm^{-1} was assigned for O–H stretching, and the peaks at 1750 and 1095 cm^{-1} were characterized for the C=O bond of the carboxylic groups (Castro et al. 2011; Amel et al. 2012). Peaks around 2900 and 1630 cm^{-1} were assigned for the C–H and C=C stretching due to the lignin containing aromatic benzene rings, respectively. Weak



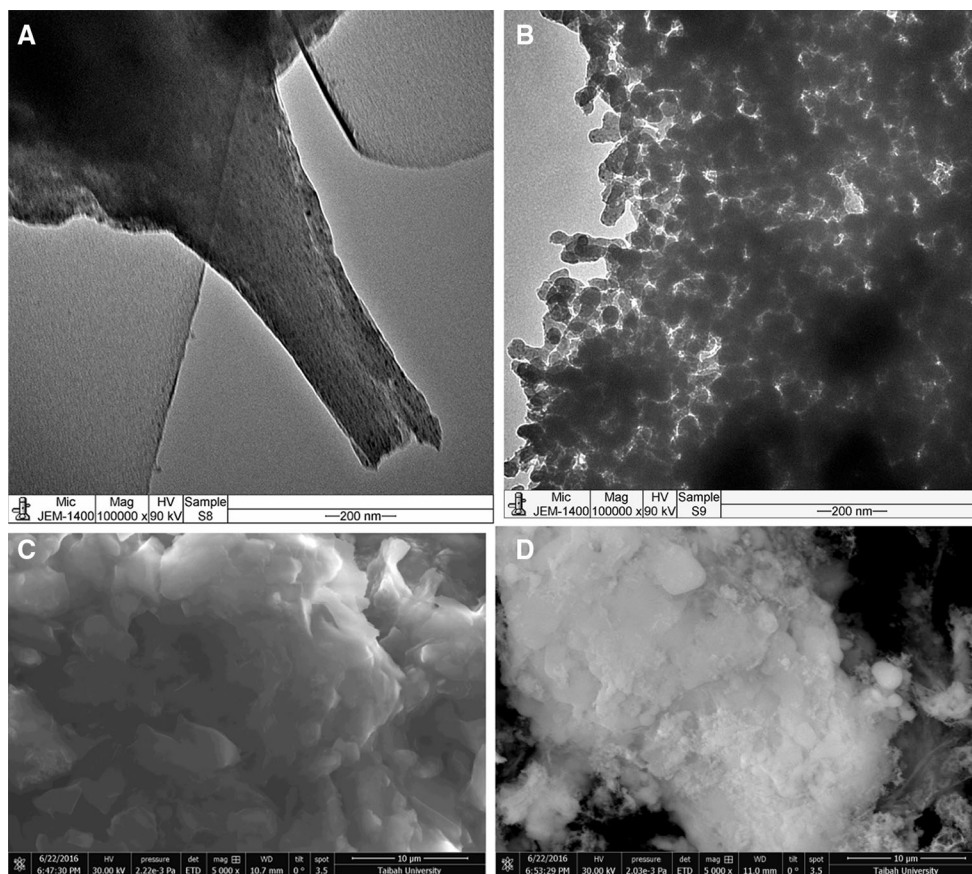


Fig. 2 Transmission electron microscope (TEM) and scanning electron microscope (SEM) images for **a, c** BP and **b, d** CSNC, respectively

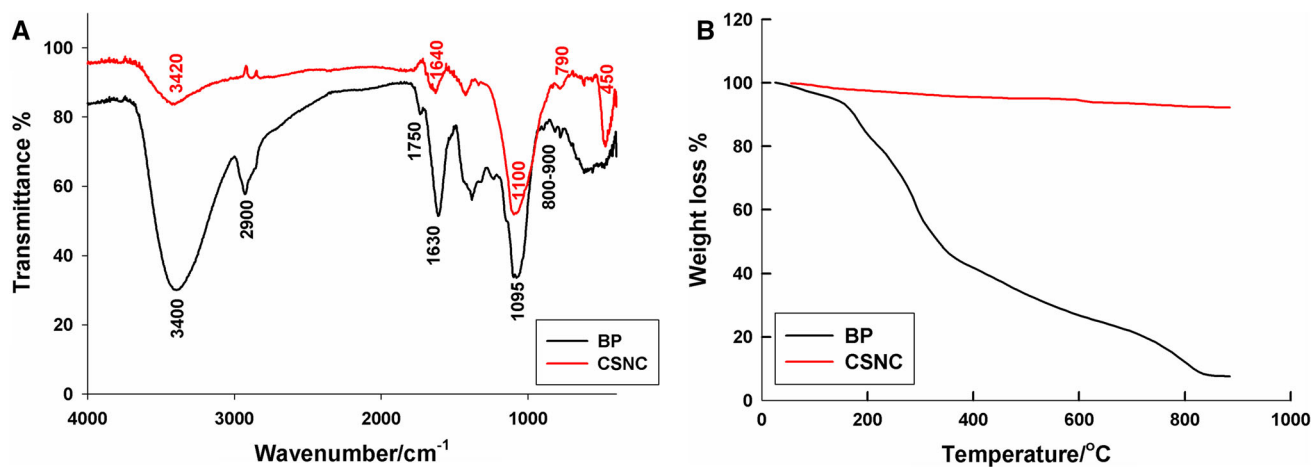


Fig. 3 **a** Fourier transform IR (FTIR) and **b** thermal gravimetric analysis (TGA) curves of BP and CSNC

bands appeared in the range of $800\text{--}900\text{ cm}^{-1}$ which were attributed to amine groups (Amel et al. 2012).

For the CSNC sample, the O–H stretching peak appeared at 3420 cm^{-1} , but it had lower intensity compared to that of the BP which indicated the decreased number of OH groups upon modification. The O–H bending peak appeared at

1640 cm^{-1} . The characteristic peaks of silica appeared at 1100 , 790 , and 450 cm^{-1} which are corresponding to Si–O–Si bonds asymmetric, symmetric stretching and bending, respectively (Ferreira et al. 2015).

Figure 3b shows thermogravimetric analysis of BP and CSNC; for natural BP, the decomposition is gradual and



starts at 160 °C. On the other hand, CSNC showed high thermal stability over the studied temperature range 25–900 °C, due to the presence of the thermally stable SiO₂ in the composite which then indicated the possibility of using CSNC for high-temperature applications.

Application of CSNC as a biosorbent for MB removal

pH effect

The point of zero charge (PZC) for CSNC was evaluated by adding 0.05 g of CSNC to 25 mL of deionized water of different pH values. The suspension solutions have been shaken for 24 h; then, the final pH values were measured (Foroughidahr et al. 2015; Kallel et al. 2016). A plot of the pH differences against initial pH values is shown in Fig. 4a. The point of intersection at $\text{pH}_f - \text{pH}_i = \text{zero}$ is corresponding to the PZC which is equal to 4.5. At this point, the sorbent has a net charge of zero; before PZC, the sorbent has positive charges, while after PZC, the sorbent has negative charges. The determination of this point is very important to elucidate the electrostatic attraction between the CSNC sorbent and the cationic MB dye. The pka value of MB dye is 0.04 (Bhatti et al. 2012), this means that above this value, the dye is completely dissociated into cationic forms. However, the proposed sensor is negatively charged at pH value of 4.5, therefore; the efficient dye uptake by the sorbent is expected to be at pH value above 4.5 due to the enhanced electrostatic attractions between the cationic dye and the negatively charged sorbent.

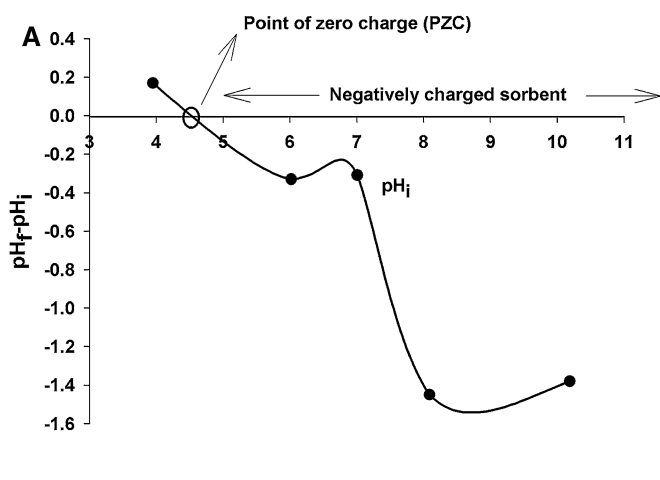
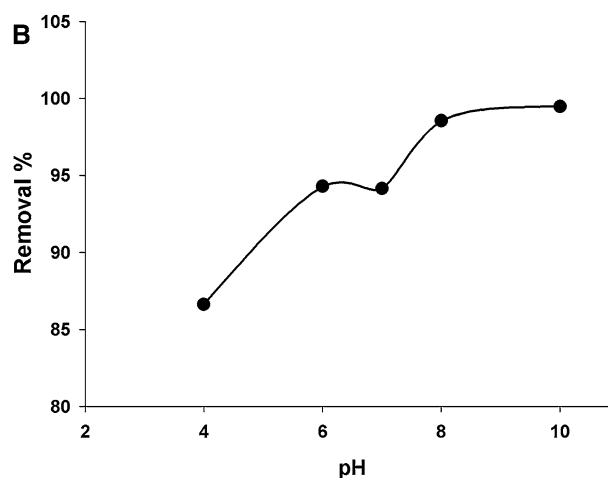


Fig. 4 **a** pH change as a function of the initial solution pH for the determination of point of zero charge (PZC) of CSNC, **b** the effect of pH on the removal % of methylene blue (MB) dye by CSNC, initial

The pH effect on the removal process of MB on CSNC is presented in Fig. 4b. The removal % of MB was slightly increased by increasing the pH from 4 to 10, from 86.5 to 99.6%. The sorbent possessed excellent removal ability at the studied pH range, and this can be due to the electrostatic attraction between the negatively charged sorbent (at $\text{pH} > 4$) and the positively charged cationic MB dye. At $\text{pH} = 4$, the removal % was slightly decreased as the sorbent become positively charged; however, other types of bonding (in addition to the electrostatic attraction) between CSNC and MB dye, such as chemical adsorption through active functional groups of CSNC, still existed and affected the adsorption process. The presence of hydroxyl groups in CSNC was ascertained by FTIR analysis as mentioned in the previous section.

Kinetics and thermodynamic study

The variation of the adsorption removal % with the contact time is presented in Fig. 5a. It is shown that about half of the dye was rapidly adsorbed the CSNC in the first few minutes; then, the removal % continued to increase gradually with time. After 2 h, about 99.5% of the MB dye had been successively adsorbed on the sorbent active sites. The pseudo-first- and pseudo-second-order equations (Ansari and Dezhampanah 2013) were applied to the kinetic data (only pseudo-second-order plot is shown in Fig. 5b). Rate constants values are 0.0361 min^{-1} and $0.0581 \text{ mg g}^{-1} \text{ min}^{-1}$ for the pseudo-first- and pseudo-second-order models, respectively. Based on the correlation coefficient (r^2) values, 0.9478 and 0.9943 for the pseudo-first- and pseudo-second-order models, respectively, the pseudo-second-order model fitted the kinetics data of the MB



dye concentration = 50 ppm, contact time = 24 h, and sorbent amount is 0.1 g/50 mL of the dye solution

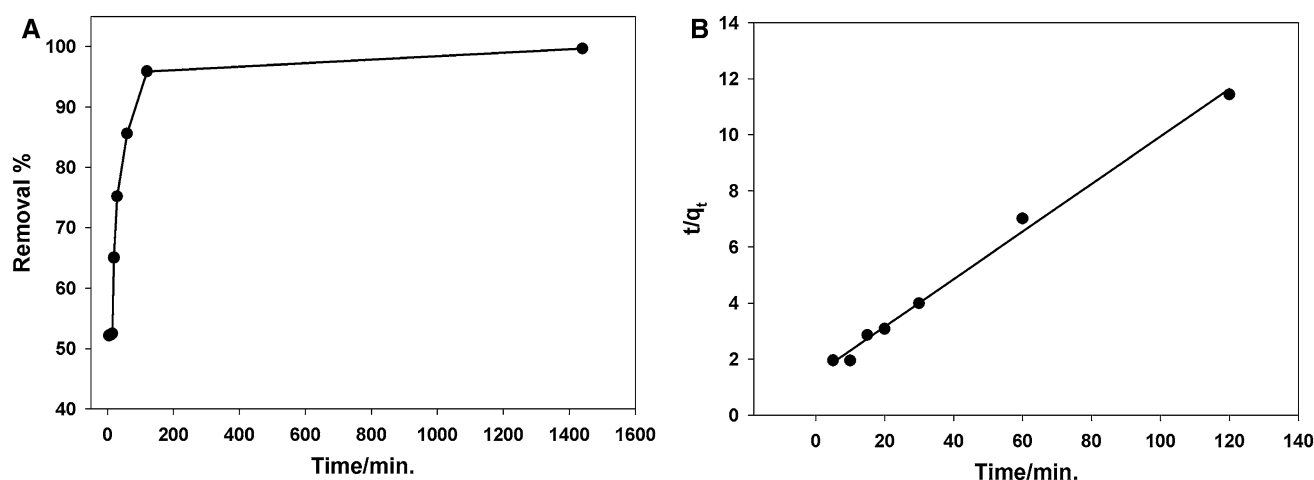


Fig. 5 **a** The variation of the removal % of MB dye on CSNC with contact time, initial dye concentration = 20 ppm at pH 7, and sorbent amount is 0.1 g/50 mL of the dye solution. **b** Pseudo-second-order kinetic model for adsorption of MB on CSNC

adsorption on CSNC better than pseudo-first-order model. Moreover, a better matching between both experimental and calculated q_e values at equilibrium, $(q_e)_{exp} = 9.89 \text{ mg g}^{-1}$, was shown in the case of the pseudo-second-order model; q_e values are 7.70 and 11.09 mg g^{-1} for the pseudo-first- and pseudo-second-order models, respectively. Data following the pseudo-second-order model indicated that the adsorption process consisted of the chemisorption interactions between CSNC and the studied MB dye (Wang et al. 2010) with initially fast physical adsorption removal (Chingombe et al. 2006; Weber and Morris 1963).

The adsorption of the MB dye on CSNC was examined at different temperatures from 288 to 328 K. Figure 6a shows the variation of the removal % of the MB with temperature. It is observed that the removal % increased sharply with the temperature rise; then, it reached a constant value, 97.9% at 318 K. The increase in the adsorption sites' number due to the bonds' break at the sorbent's surface can be a possible reason for the increased adsorption with temperature (He and Huang 1985).

Values of the thermodynamic parameters, entropy (ΔS), enthalpy (ΔH), and Gibbs free energy (ΔG) changes are calculated from the transition-state plot, shown in Fig. 6b, and listed in Table 1 (Ansari and Dezhmanpanah 2013).

$$\Delta G = \Delta H - T\Delta S \quad (10)$$

The endothermic adsorption process and the increased randomness during the uptake of the MB dye onto the CSNC sorbent were proved by the positive signs of ΔH and ΔS , respectively.

The spontaneous adsorption process is ascertained by the negative (ΔG) sign. Values become more negative with the rising of temperatures, indicating that the adsorption is

more favored with the temperature which is a sign of chemical adsorption (Marcus 1991; Pan et al. 2005).

The adsorption activation energy can be estimated by calculating the pseudo-second-order rate constants at different temperatures and then applying the Arrhenius plot (Al-Rashed and Al-Gaid 2012), shown in Fig. 6c. The activation energy value is $77.28 \text{ kJ mol}^{-1}$, suggesting a chemisorption mode (greater than 40 kJ mol^{-1}) (Wu et al. 2009; Kavitha and Namasivayam 2007).

Effect of sorbent loading

Various amounts of the CSNC sorbent, ranging between 0.025 and 0.300 g/50 mL of the 80-ppm dye solution, were used in the adsorption experiment. Figure 7 shows the variation of the removal percentage of the MB dye on the CSNC with the sorbent loading; the obtained results displayed that the percentage removal of the dye increases as adsorbent loading increases. This can be due to the increased number of active sites. Then, it reached an optimum value after which no further increase in the value of the removal % can be observed. The optimum sorbent loading for the adsorption, in the investigated range, is 0.200 g of CSNC/50 mL of the dye solution.

Adsorption mechanism and real sample analysis

The adsorption test was performed at different initial dye concentrations, and the variation of the removal % and the amount of the dye adsorbed as a function of the initial MB concentration is given in Fig. 8a. High and constant removal % has been observed, 98%, at any dye concentration, and the amount of the dye adsorbed (q_e) increases with increasing the initial dye concentration which reflects the high sorption ability of the CSNC for the MB dye.

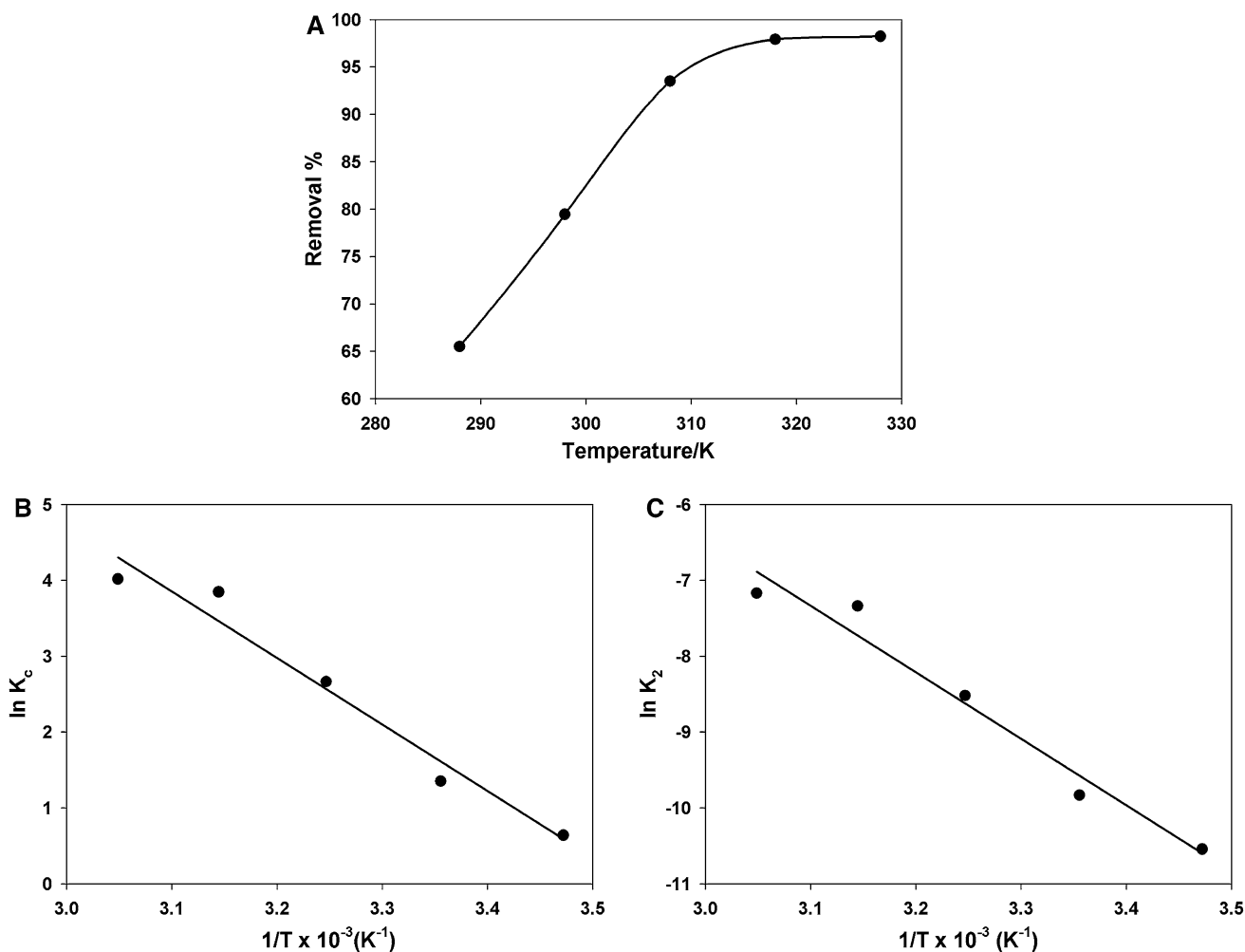


Fig. 6 **a** Variation of the removal % of MB by CSNC with temperature, initial dye concentration = 20 ppm at pH 7, and sorbent amount is 0.1 g/50 mL of the dye solution. **b** Transition-state and **c** Arrhenius plots

Table 1 Calculated thermodynamics parameters for adsorption of MB dye on cellulose/SiO₂ nanocomposite (CSNC)

ΔH (kJ mol ⁻¹)	ΔS (kJ mol ⁻¹ K)	$-\Delta G$ (kJ mol ⁻¹)				
		288 K	298 K	308 K	318 K	328 K
72.78	0.26	1.53	3.34	6.82	10.16	10.94

Langmuir and Freundlich models can be used to elucidate the adsorption mechanism (Jebreil 2014; Dawood and Sen 2012). Both models were applied to the adsorption data as indicated in Fig. 8b, c. Adsorption isotherms parameters, Langmuir maximum adsorption capacity (q_m), Langmuir constant (b) and Freundlich’s constants (K_f and n), were calculated ($q_m = 78.75 \text{ mg g}^{-1}$, $b = 2.07 \text{ L mg}^{-1}$, $K_f = 18.17 \text{ mg g}^{-1}$, and $n = 1.45 \text{ g L}^{-1}$). According to the values of the correlation coefficients, $r^2 = 0.9982$ and 0.9851 for Langmuir and Freundlich isotherms, respectively, Langmuir model can be employed to fit data better

than Freundlich model. Langmuir isotherm indicated that the adsorption of the adsorbate occurs on homogeneous adsorbent. The maximum adsorption capacity value (q_m) for the removal of the MB dye by CSNC is 78.75 mg g^{-1} , while the value reported for the untreated BP was 21 mg g^{-1} (Annadurai et al. 2002) which means that adsorption capacity is enhanced by about four times. Table 2 shows a comparison of sorption capacity values of other nanosorbents reported for the MB removal. It can be shown that the proposed sorbent, CSNC, has a moderate sorption capacity; however, its low cost and facile

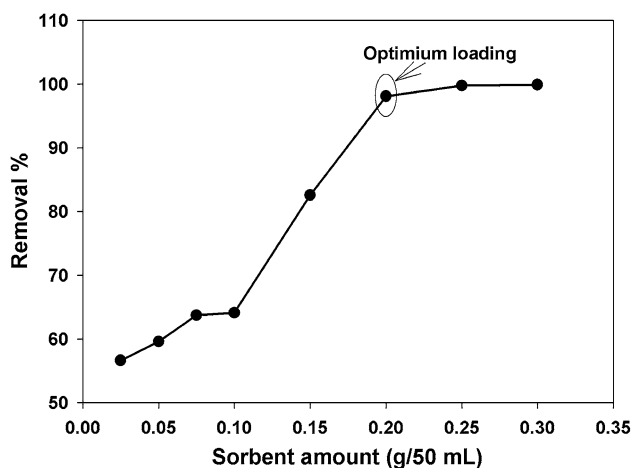


Fig. 7 Variation of the removal % of MB dye on CSNC with the sorbent loading, initial dye concentration = 20 ppm at pH 7

preparation would contribute to its usage. It is recommended in the future study to investigate the performance of other agricultural wastes nanocomposites, change the supporting nanooxide type, and optimize the synthesis conditions so that the sorption capacity value may be further enhanced.

The adsorption capacity of the CSNC for MB was also determined in wastewater sample to examine the matrix effect. Different initial MB concentrations (5–100 ppm) were prepared in wastewater (taken from one drainage basin in Madinah, KSA); then, the adsorption test was performed. A correlation coefficient (r^2) value of 0.9873 was obtained, and the maximum adsorption capacity was 58.81 mg g^{-1} . It can be concluded that the CSNC still shows a comparable adsorption capacity for the MB in the real sample to that in aqueous solutions which promotes its use in field applications.

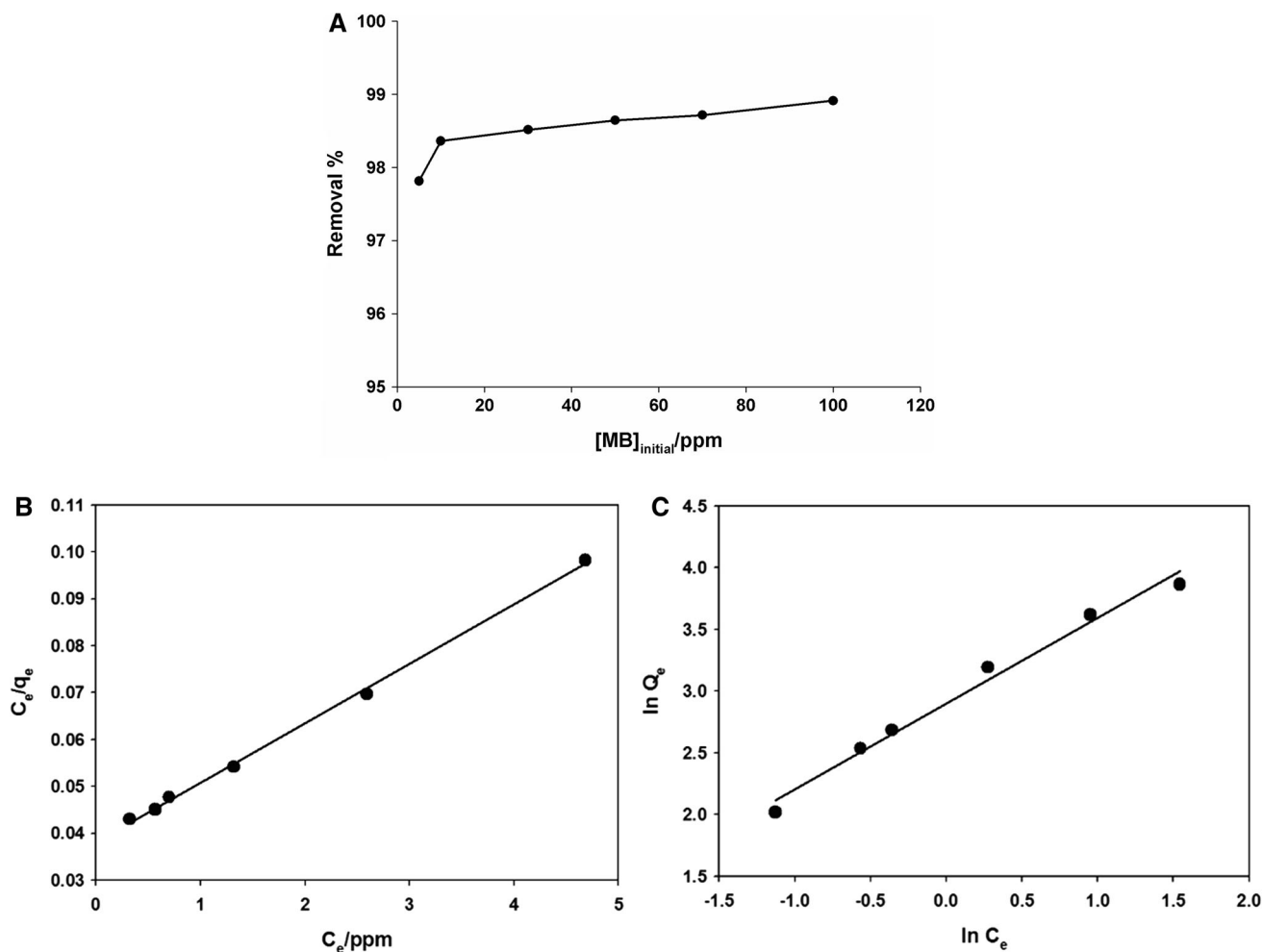


Fig. 8 a Variation of the removal % of MB dye on CSNC with the initial MB dye concentration, at pH 7, and sorbent amount is 0.1 g/50 mL of the dye solution. b Langmuir and c Freundlich adsorption isotherms



Table 2 A comparison of the adsorption capacity of CSNC with other nanosorbents reported in the literature for methylene blue removal

Nanosorbent	Maximum adsorption capacity (q_m , mg g ⁻¹)	References
Fe ₂ O ₃ /SiO ₂	26.62	Chen et al. (2016)
Fe ₃ O ₄ /graphene/SiO ₂	139.64	Wu et al. (2016b)
γ -Fe ₂ O ₃ /graphene	216.3	Song et al. (2015)
MIL-100(Fe)	1105	Tan et al. (2015)
graphene-Fe ₃ O ₄ /calcium alginate	17.27	Zhang et al. (2016)
Zn ₃ [Fe(CN) ₆] ₂ ·xH ₂ O	1016	Wu et al. (2016a)
CSNC	78.75	This study

Conclusion

- Cellulose/SiO₂ nanocomposite can be successively prepared by a template-assistant synthesis method using natural banana peel waste as a template for nanosilica.
- XRD proved the formation of the composite with silica as the main phase, and an average particle size of about 20 nm, as shown by TEM image of the nanocomposite.
- BET surface area and the thermal stability have been enhanced upon the composite formation, with respect to natural banana peel.
- Cellulose/SiO₂ nanocomposite can be applied as a biosorbent for the removal of methylene blue from aqueous solutions and wastewater with sorption capacity values of 78.75 and 58.81 mg g⁻¹, respectively, suggesting the applicability of the proposed sorbent for field uses.
- The adsorption follows pseudo-second-order model, indicating chemisorption interactions between the nanocomposite and the studied dye with initially fast physical adsorption. The activation energy value is 77.28 kJ mol⁻¹, ascertaining a chemisorption mode.
- The adsorption is endothermic and spontaneous and follows Langmuir isotherm.

Acknowledgements Author is grateful to the University of Taibah for the availability of measuring and analysis instruments.

References

- Ali A (2017) Removal of Mn(II) from water using chemically modified banana peels as efficient adsorbent. *Environ Nanotech Monit Manag* 7:57–63
- Ali A, Saeed K, Mabood F (2016) Removal of chromium (VI) from aqueous medium using chemically modified banana peels as efficient low-cost adsorbent. *Alex Eng J* 55:2933–2942
- Al-Rashed SM, Al-Gaid AA (2012) Kinetic and thermodynamic studies on the adsorption behavior of rhodamine B dye on duolite C-20 resin. *J Saudi Chem Soc* 16:209–215
- Amel K, Hassena MA, Kerroum D (2012) Isotherm and kinetics study of biosorption of cationic dye onto banana peel. *Energy Procedia* 19:286–295
- Anastopoulos I, Kyzas GZ (2014) Agricultural peels for dye adsorption: a review of recent literature. *J Mol Liq* 200:381–389
- Anastopoulos I, Kyzas GZ (2015) Composts as biosorbents for decontamination of various pollutants: a review. *Water Air Soil Pollut* 226:61
- Annadurai G, Juang RS, Lee DJ (2002) Use of cellulose-based wastes for adsorption of dyes from aqueous solutions. *J Hazard Mater* 92:263–274
- Ansari R, Dezhampanah H (2013) Application of polyaniline/sawdust composite for removal of acid green 25 from aqueous solutions: kinetics and thermodynamic studies. *Sect B-Res Pap* 25:220–225
- Bhatti HN, Akhtar N, Saleem N (2012) Adsorptive removal of methylene blue by low-cost citrus sinensis bagasse: equilibrium, kinetic and thermodynamic characterization. *Arab J Sci Eng* 37:9–18
- Cao J, Rambo CR, Sieber H (2004) Preparation of porous Al₂O₃-ceramics by biotemplating of wood. *J Porous Mater* 11:163–172
- Carvalho HP, Huang J, Zhao M, Liu G, Dong L, Liu X (2015) Improvement of methylene blue removal by electrocoagulation/banana peel adsorption coupling in a batch system. *Alex Eng J* 54:777–786
- Castro RSD, Caetano L, Ferreira G, Padilha PM, Saeki MJ, Zara LF, Martines MAU, Castro GR (2011) Banana peel applied to the solid phase extraction of copper and lead from river water: preconcentration of metal ions with a fruit waste. *Ind Eng Chem Res* 50:3446–3451
- Chen D, Zeng Z, Zeng Y, Zhang F, Wang M (2016) Removal of methylene blue and mechanism on magnetic γ -Fe₂O₃/SiO₂ nanocomposite from aqueous solution. *Water Resour Ind* 15:1–13
- Chingombe P, Saha B, Wakeman RJ (2006) Sorption of atrazine on conventional and surface modified activated carbons. *J Colloid Interface Sci* 302:408–423
- Crini G (2006) Non-conventional low-cost adsorbents for dye removal: a review. *Bioresour Technol* 97:1061–1085
- Dawood S, Sen TK (2012) Removal of anionic dye congo red from aqueous solution by raw pine and acid-treated pine cone powder as adsorbent: equilibrium, thermodynamic, kinetics, mechanism and process design. *Water Res* 46:1933–1946
- Ferreira CS, Santos PL, Bonacin JA, Passos RR, Pocrifk LA (2015) Rice husk reuse in the preparation of SnO₂/SiO₂ Nanocomposite. *Mater Res* 18:639–643
- Foroughidahr M, Abolghasemi H, Esmaili M, Nazari G, Rasem B (2015) Experimental study on the adsorptive behavior of congo red in cationic surfactant-modified tea waste. *Process Saf Environ* 95:226–236
- Gong R, Ding Y, Li M, Yang C, Liu H, Sun Y (2005) Utilization of powdered peanut hull as biosorbent for removal of anionic dyes from aqueous solution. *Dyes Pigments* 64:187–192
- Hameed BH (2009) Grass waste: a novel sorbent for the removal of basic dye from aqueous solution. *J Hazard Mater* 166:233–238



- Hashemian S, Foroghmoqhadam A (2014) Effect of copper doping on CoTiO₃ ilmenite type nanoparticles for removal of congo red from aqueous solution. *Chem Eng J* 235:299–306
- He BL, Huang WQ (1985) Ion exchanger and adsorptive resin. Shanghai Sci Technol Press, Shanghai
- Jebreil SA (2014) Removal of tartrazine dye from aqueous solutions by adsorption on the surface of polyaniline/iron oxide composite. *Int Sch Sci Res Innov* 8:1346–1351
- Kallel F, Chaari F, Bouaziz F, Bettaieb F, Ghorbel R, Chaabouni SE (2016) Sorption and desorption characteristics for the removal of a toxic dye, methylene blue from aqueous solution by a low cost agricultural by-product. *J Mol Liq* 219:279–288
- Kavitha D, Namasivayam C (2007) Experimental and kinetic studies on methylene blue adsorption by coir pith carbon. *Bioresour Technol* 98:14–21
- Kumar KV, Kumaran A (2005) Removal of methylene blue by mango seed kernel powder. *Biochem Eng J* 27:83–93
- Kyzas GZ, Matis KA (2015) Nano-adsorbents for pollutants removal: a review. *J Mol Liq* 203:159–168
- Mamoru M, Haruyuki T, Nobuyasu A, Toshitaka O, Keiji D, Yasuo H (2005) Porous ceramics prepared by mimicking silicified wood. *Sci Technol Adv Mater* 6:76–83
- Marcus Y (1991) Thermodynamics of solvation of ions: part 5-Gibbs free energy of hydration at 298.15 K. *J Chem Soc Faraday Trans* 87:2995–2999
- Nagendra PS, Prasad VVS, Ramji K, Pusty G (2014) Synthesis of Bio-degradable banana nanofibers. *Int J Innov Tech Res* 2:730–734
- Ota T, Imaeda M, Takase H, Kobayashi M, Kinoshita N, Hirashita T, Miyazaki H, Hikichi Y (2000) Porous titania ceramic prepared by mimicking silicified wood. *J Am Ceram Soc* 83:1521–1523
- Pan BC, Zhang QX, Meng FW (2005) Sorption enhancement of aromatic sulfonates onto an aminated hyper-cross-linked polymer. *Environ Sci Technol* 39:3308–3313
- Pang SC, Chin SF, Yih V (2011) Conversion of cellulosic waste materials into nanostructured ceramics and nanocomposites. *Adv Mat Lett* 2:118–124
- Patel M, Padhi BK (1993) Titania fibres through jute substrates. *J Mater Sci Lett* 12:1234–1235
- Pereira PHF, Benini KCC, Watashi CY, Voorwald HJC, Cioffi MOH (2013) Characterization of high density polyethylene (HDPE) reinforced with banana peel fibers. *Bioresources* 8:2351–2365
- Pillai SS, Deepa B, Abraham E, Giriya N, Geetha P, Jacob L, Koshy M (2013) Biosorption of Cd(II) from aqueous solution using xanthated nanobanana cellulose: equilibrium and kinetic studies. *Ecotoxicol Environ Saf* 98:352–360
- Rao KS, Khalil EH, Kodaki T, Matsushige K, Makino K (2005) A novel method for synthesis of silica nanoparticles. *J Colloid Interface Sci* 289:125–131
- Song N, Wu X, Zhong S, Lin H, Chen J (2015) Biocompatible γ -Fe₃O₄/CA nanocomposites for the removal of methylene blue. *J Mol Liq* 212:63–69
- Tan F, Liu M, Li K, Wang Y, Wang J, Guo X, Zhang G, Song C (2015) Facile synthesis of size-controlled MIL-100(Fe) with excellent adsorption capacity for methylene blue. *Chem Eng J* 281:360–367
- Thuan TV, Quynh BTP, Nguyen TD, Ho VTH, Giang L (2017) Response surface methodology approach for optimization of Cu²⁺, Ni²⁺ and Pb²⁺ adsorption using KOH-activated carbon from banana peel. *Surf Interface* 6:209–217
- Tibolla H, Pelissari FM, Menegalli FC (2014) Cellulose nanofibers produced from banana peel by chemical and enzymatic treatment. *LWT-Food Sci Technol* 59:1311–1318
- Vadivelan V, Kumar KV (2005) Equilibrium, kinetics, mechanism, and process design for the sorption of methylene blue onto rice husk. *J Colloid Interface Sci* 286:90–100
- Wang XS, Chen LF, Li FY, Chen KL, Wan WY, Tang YJ (2010) Removal of Cr(VI) with wheat-residue derived black carbon: reaction mechanism and adsorption performance. *J Hazard Mater* 175:816–822
- Weber WJ, Morris JC (1963) Kinetics of adsorption on carbon from solution. *J Sanit Eng Div Am Soc Civ Eng* 89:31–60
- Wu FC, Tseng RL, Juang RS (2009) Initial behavior of intraparticle diffusion model used in the description of adsorption kinetics. *Chem Eng J* 153:1–8
- Wu S, Shen X, Zhou H, Zhu G, Wang R, Ji Z, Chen K, Chen C (2016a) Morphological synthesis of prussian blue analogue Zn₃[Fe(CN)₆]₂·xH₂O micro-/nanocrystals and their excellent adsorption performance toward methylene blue. *J Colloid Interface Sci* 464:191–197
- Wu X, Shi Y, Zhong S, Lin H, Chen J (2016b) Facile synthesis of Fe₃O₄-graphene@mesoporous SiO₂ nanocomposites for efficient removal of methylene blue. *Appl Surf Sci* 378:80–86
- Zhang LY, Zhang W, Zhou Z, Li CM (2016) γ -Fe₂O₃ nanocrystals-anchored macro/meso-porous graphene as a highly efficient adsorbent toward removal of methylene blue. *J Colloid Interface Sci* 476:200–205

